HHS Public Access

Author manuscript

ACS Biomater Sci Eng. Author manuscript; available in PMC 2024 March 13.

Published in final edited form as:

ACS Biomater Sci Eng. 2023 March 13; 9(3): 1644–1655. doi:10.1021/acsbiomaterials.2c01370.

Membrane remodeling of Human Engineered Cardiac Tissue by Chronic Electric Stimulation

Alberto Sesena-Rubfiaro[1], **Navin J. Prajapati**[1], **Lia Paolino**[2], **Lihua Lou**[3], **Daniel Cotayo**[1], **Popular Pandey**[1], **Mohammed Shaver**[2], **Joshua Hutcheson**[2,4], **Arvind Agarwal**[3], **Jin He**[1,4,*]

[1]Department of Physics, Florida International University, Miami, FL 33199, USA

[2]Department of Biomedical Engineering, Florida International University, Miami, FL 33199, USA

[3]Department of Mechanical and Materials Engineering, Florida International University, Miami, FL 33174, USA

[4]Biomolecular Science Institute, Florida International University, Miami FL 33199, USA

Abstract

Human-induced pluripotent stem cell–derived cardiomyocytes (hiPSC-CMs) show immature features, but these are improved by integration into 3D cardiac constructs. In addition, it has been demonstrated that physical manipulations such as electrical stimulation (ES) are highly effective in improving the maturation of human-engineered cardiac tissue (hECT) derived from hiPSC-CMs. Here, we continuously applied a ES in capacitive coupling configuration, which is below the pacing threshold, to millimeter size hECTs for 1–2 weeks. Meanwhile, the structural and functional developments of the hECTs were monitored and measured using an array of assays. Of particular note, a nanoscale imaging technique, scanning ion conductance microscope (SICM) has been used to directly image membrane remodeling of CMs at different locations on the tissue surface. Periodic crest/valley patterns with a distance close to the sarcomere length appeared on the membrane of CMs near the edge of the tissue after ES, suggesting the enhanced transverse tubulation network. The SICM observation is also supported by the fluorescence images of transverse tubulation network and α-actinin. Correspondingly, essential cardiac function such as calcium handling and contraction force generation were improved. Our study provides evidence that chronic subthreshold ES can still improve the structural and functional developments of hECTs.

Graphical Abstract

[*]**Corresponding Author**: **Jin He** – Physics department, Biomolecular Science Institute, Florida International University, Miami FL 33199, USA, jinhe@fiu.edu.

Author Contributions

A.S.-R.: Investigation, Formal analysis, Writing an original draft. N.J.P., L.P.: Investigation, Methodology. L.L., D.C., P.P.: Investigation, Methodology. M.S.: Methodology. J.H.: Resources, Methodology. A.A.: Investigation, Methodology, Supervision. J.H.: Investigation, Methodology, Supervision, Conceptualization, Funding, Writing a draft.

Supporting Information

The Supplementary Information is available free of charge *via* the Internet at https://pubs.acs.org/doi/10.1021/acsbiomaterials.2c01370.

The authors declare no competing financial interest in association with this study.

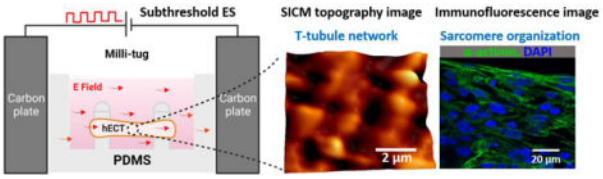

The subthreshold electrical stimulation in capacitive coupling configuration can improve the maturation of the human engineered cardiac tissue (hECT) and induce structural development of the t-tubule system on the cardiomyocyte membrane, as revealed by the topography images of scanning ion conductance microscopy and the immunofluorescence images of sarcomere.

Keywords

cardiomyocytes; engineered cardiac tissue; electric stimulation; scanning ion conductance microscopy; indentation

Introduction

Despite marked progress in medical treatment, myocardial infarction remains a major health and socio-economic burden associated with high mortality rate. Studies in adult human hearts show a renewed capacity of cardiomyocytes (CMs) after injury; however, the spontaneous turnover rate of CMs cannot lead to meaningful functional recovery[1]. Human-induced pluripotent stem cells (hiPSCs) are proposed as an unlimited source of CMs that, in theory, would lead the development of a functional human cardiac tissue for basic research and regenerative medicine. However, these cells do not exhibit all the properties that represent adult human CMs. Rather, they display immature features such as poor sarcomere alignment, low myofibril volume, early fetal gene expression profile, and unregulated intracellular calcium handling, to name a few[2]. Therefore, the maturation of hiPSC-CM is required to achieve appropriate physiological characteristics that enable the development of tissue models for cardiac regeneration studies[3].

To achieve a higher degree of maturation, a variety of methods have been developed. For example, with prolonged culture time in 2D environment, hiPSC-CMs displayed more mature features such as larger cell size, better sarcomere alignment and the improvement in calcium handling[4, 5]. Replanting of hiPSC-CMs from stiffer substrate (culture dish ~1MPa) to soft polydimethylsiloxane(PDMS) substrate with stiffness close to human heart (~10kPa) can lead to a better maturation process[6]. Mimicking the stiffness of the natural extracellular matrix (ECM) and improving their electrical properties with nanomaterials promote engineered cardiac tissue (ECT) maturity, excitability and electrical signal propagation[7]. Moreover, other methods include dynamic culture to enhance the transport of nutrients and oxygen[8], the addition of growth factors into the cell medium culture by the co-culture with mesenchymal stem cells or the addition of oxidative substrates adapted to the metabolic needs of the hiPSC-CMs[9], 3D printing cardiac organoids with embedded vascular channels and 3D engineered cardiac constructs that promote the alignment and electromechanical coupling[10, 11]. Physical training methods, such as mechanical stimulation, can also promote hiPSC-CM maturation, with cyclic mechanical

stress applied by external stretching devices to force the assembly of muscle-cells into structurally and functionally aligned 3D structures[10, 12]. Furthermore, electrical pacing on ECTs has been shown to greatly improve the maturation process by upregulating cardiac markers, promoting sarcomere alignment, increasing the contractile force, and improvement of calcium handling[13–15]. Ultrastructural analysis of the engineered cardiac tissues under electrical pacing has revealed the development of transverse tubules (t-tubules). These critical and highly complex compartments act as a framework for many of the proteins involved in the excitation-contraction coupling.

In this report, we studied the effect of electrical stimulation (ES) below the pacing threshold on the development of hECTs. As shown in Figure 1A, the hECTs are formed from early-stage hiPSC-CMs shortly after the initiation of spontaneous contractions, following previously reported procedures[15]. The hiPSC-CMs are mixed with fibrin hydrogel components and Matrigel in a millimeter size well containing two flexible PDMS posts (referred to hereafter as milli-tug device). After matrix polymerization and CMmediated contraction, the mixture forms a hECT suspended between two posts, which providing the static mechanical load (see Figure 1B). The typical size of the tissue is approximately 1.5 mm in length, 0.28 mm in thickness, and 0.6 mm for the narrowest width in the middle (see Figure 1B (iii)). The narrower width in the middle is mainly due to the relative tension differences in the matrix[16]. ES with monophasic square wave pulses at 5 Hz is applied between two carbon plates in the capacitive coupling configuration (see Figure 1B(ii)). Compared with the direct coupling configuration, this configuration is convenient to use and can avoid unwanted electrochemical reactions and heating problems induced by the direct contact between the electrode and electrolyte[17], which is beneficial for long-term usage inside the incubator. The downside of this method is the limited magnitude of the electric field. Here, the applied electric field magnitude is about 5–10 times smaller than the typical value used for supra-threshold electrical pacing in direct coupling configuration for hECTs.

To characterize the ultrastructural improvements, we have used a new imaging technique, scanning ion conductance microscopy (SICM)[18], capable of imaging the topography changes of cell surface in physiological conditions with nanoscale resolution. SICM has been successfully applied to study the t-tubules system of isolated CMs from adult rat and human heart tissues[19–21]. T-tubules are membrane organelles that consist of sarcolemma penetrating the interior of CMs, forming a highly branched and interconnected network. These structures permit the efficient transmission of the electrical signal giving the synchronization of intracellular calcium release, which causes the contraction of the tissue[22]. The periodic surface patterns of the mature t-tubule system can be resolved in the topography images by SICM. However, the previous studies are all based on individual CMs isolated from matured heart tissues. In this work, we successfully applied SICM to directly image the membranes of CMs on the surface of the developing hECTs. We observed the continuous membrane remodeling of CMs in the hECT suggesting the development of the t-tubule network. More obvious surface patterns have been observed in the ones after applied ES. By imaging CMs at different locations of the hECT, we also observed obvious heterogeneity in membrane modeling, which is attributed to the tension distribution in the suspended hECT. The SICM results are supported by other structural and functional measurements. Therefore, a mild ES is still beneficial for the development of hECT.

2. Methods

2.1 Cardiac differentiation of HiPSCs

The preparation of hiPSCs is illustrated in Figure 1A. The hiPSCs from reprogrammed fibroblasts (GM23338, Coriell Institute for Medical Research, NJ, USA) were delivered and stored in liquid nitrogen until use. After defrosting, cells were cultured according to a previously described protocol[23]. Briefly, hiPSC cells were cultured on Matrigel-coated plates (BD Biosciences) with stem basal medium (mTeSR1, STEMCELL Technologies) for about 5 days to reach 80–90% of confluence. On day 0, hiPSCs were treated with 12 μM CHIR99021 (Tocris, 4423) diluted in RPMI/B27 minus insulin for 24 hours. On day 3, hiPSCs were treated with 5 μM IWP4 (Tocris, 5214) mixed with RPMI/B27 minus insulin, removed on day 4. The medium was changed every other day. From day 8, hiPSCs were maintained in RPMI/B27 containing insulin with regular medium change. Spontaneous contractions were observed between days 8 and 10. Following the previously reported protocol[24], to increase the percentage of CMs, on the first day of beating, the hiPSCs were treated with the Lactate medium, with 5mM L-Lactate (Sigma, 71718) diluted in RPMI without glucose (Gibco, 11879–020), for 3 days. The medium was replaced daily.

2.2 The formation of HECTs

Lactate purified hiPSC-CMs were dissociated from the substrate by TrypLE Express solution (Gibco) at 37 °C for 15 min. The detached cells were collected by centrifugation at 1000 RPM for 6 min. It has previously been demonstrated that different hydrogels such as collagen and fibrin can support the assembly of functional cardiac tissues[25, 26]. Here, hiPSC-CMs were encapsulated in the ECM formed by the hydrogel mixture of fibrin and Matrigel. Each well of the PDMS milli-tug device (see below) with two flexible posts was loaded with 200,000 cells in a suspension of 2 μL RPMI/B27, 1.23 μL of human fibrinogen (Sigma, F3879), 0.2 μL of human thrombin (Sigma, 605190-M), and 0.6 μL of Matrigel (Corning, 356230). Then the device was filled with 35 μL of RPMI/B27 containing insulin, 5 μM Y27632 (Tocris, 1254), 10% fetal bovine serum, and 0.033 mg/mL aprotinin (Sigma, A3428). The medium was changed every other day. The tissue was formed from day 17, and spontaneous beating was observed between days 19–20. The cells in the tissue at that time were not synchronized. Synchronous contraction of the tissue required approximately two additional days.

2.3 The fabrication of milli-tug device

Milli-tug devices (see Figures 1B and 1C) were fabricated by first pouring uncured PDMS (Dow Corning Sylgard 184 prepared at 25:1 ratio of base: curing agent) into a polypropylene mold, which was then baked overnight at 70 °C. Before cell seeding, the milli-tug devices were sterilized by immersion in 70% ethanol for 30 minutes and exposure to UV-light for 20 minutes[25]. The surfaces of the device were treated with 2% Pluronic F127 to reduce cell adhesion. The final milli-tug device presents two posts with hemispherical caps of 0.39 mm diameter, 1.46 mm height, and 0.39 mm thickness.

2.4 Twitch force measurement

The spontaneous contraction force (twitch force) and the corresponding beating frequency was measured based on the deflection of flexible post top (Δx) in the milli-tug device, as previously described[27]. Briefly, assuming the post has uniform material properties and dimensions, each deflection reports the force contraction proportional to the post's spring constant. To calculate the twitch force (F), the spring constant (k) of the post was measured using the indentation setup (Hyditron Biosoft, Bruker, Billerica, MA) with a spherical probe of 400 μm diameter. We have found that the tissue can be located at the middle of the post from top to bottom. Therefore, the acquired spring constant k at the middle of the post was 4.47 ± 0.31 Nm^{-1} based on five measurements in air (see supplementary information Figure S1). This value was used to calculate the twitch force using equation 1.

$$F = k^{*}\Delta x . \quad \text{(Equation 1)}$$

2.5 SICM setup and imaging

The SICM setup (see Figure 2A) was based on a commercial system (XE-Bio system, Park system Inc Santa, CA) and mounted on the stage of an inverted optical microscope (Nikon Elipse Ti-U). Quartz nanopipettes were used as the scanning probes, which were prepared from capillaries (O.D. 1.2 mm, I.D. 0.90 mm, Sutter Instruments USA) by a pipette puller (P-2000, Sutter Instruments) with the following parameters: HEAT = 805, FIL = 3, VEL = 40, DEL = 220, PUL = 165. The nanopore diameter at the nanopipette tip was ~200 nm, and the nanopipette was filled with 1xPBS solution from the backend before imaging. The nanopipette was connected to a low noise current amplifier (DLPCA200, FEMTO) with a 10^9 gain. The measured ionic current was used as feedback to control the vertical distance of the nanopipette tip from the surface[28]. The SICM was operated in the approach-retraction scan (ARS) mode[29] (also called hopping mode[30]) to acquire the topography images of the cell/tissue surface. The topography image resolution was ~100 nm/pixel with the typical setting here. The time to acquire an image of 128 ×128 pixels was about 25 min. The typical setpoint is a 1% decrease of the baseline current. The tip-approaching speed during the fine scan was about 75 μm/s, and the actual current change was about 8.2%. To avoid motion artifacts during imaging, the hECTs were freshly fixed by exposing them to 1% paraformaldehyde for 2 min and rinsed 2 times in1xPBS at room temperature.

2.6 Immunofluorescence imaging of sarcomere structure

The hECTs were fixed with 4% paraformaldehyde in PBS and permeabilized with 0.2% Triton X-100 in PBS for 40 min. Then, the hECTs were rinsed in PBS for 5 min and incubated in blocking solution 1% bovine serum albumin (BSA) in PBS for 1 h. The hECTs were incubated overnight with primary antibody anti-sarcomeric α-actinin (mouse monoclonal, 1:200; Abcam ab9465) diluted in 1% BSA. On the next day, the hECTs were rinsed for 5 min in PBS and incubated with a secondary antibody for 2 h: anti-mouse IgG–Alexa Fluor 488 (1:400; Invitrogen A21202). Subsequently, the hECTs were incubated for 10 min with 4', 6-diamidino-2-phenylindole (DAPI, Invitrogen, 30 nM) and rinsed in PBS for 5 min. Fluorescence images were acquired using a Nikon C1 confocal microscope

equipped with a 60x objective and Nikon NIS Elements software. At least three regions of interest (ROIs) were imaged per biological replicate and two biological replicates were used for each condition. For quantitative analysis of the sarcomere length, a total of 20 images at different ROIs and focus depths were used. Each image contained at least 4 sarcomere lengths and an average value of sarcomere length was first obtained from each image.

2.7 Imaging of calcium transients

Tyrode solution was prepared with the following composition: NaCl 134 mM, KCl 2.68 mM, $MgCl_2$ 1.05 mM, $CaCl_2$ 1.80 mM, NaH_2PO_2 400 μM, $NaHCO_3$ 12 mM, Glucose 5.56 mM. The pH was adjusted with NaOH to reach 6.5. The chemicals were purchased from Fisher Chemical and Sigma-Aldrich. All solutions were prepared using deionized water (~18 MΩ) either from a water purification system (Ultra Purelab system, ELGA/Siemens) or purchased from Thermo Scientific (AA36645K7). Spontaneous Ca^{2+} release activity of the hECTs was monitored with Ca^{2+} sensitive fluorescent dye Fluo-4 (10 mM Fluo-4 AM) diluted in Tyrode solution for 45 min near 32 °C. A scientific CMOS camera recorded spontaneous Ca^{2+} transients at 15 frames per second (Thorlabs, CS2100M). Custom Matlab script was used to analyze the video's temporal changes of the fluorescence intensity at different ROIs. The intensity of each frame was normalized to a background baseline recorded without the sample. Ca^{2+} dynamics were quantified by computing time to peak intensity, time to 90% decay of Ca^{2+} signal intensity, and full width at halfmaximum of the Ca^{2+} transient. The calcium transients were recorded from at least three different ROIs per biological replicate and two biological replicates were used for each condition. For the quantitative analysis of the calcium dynamics, a total of 50 transients were used per condition.

2.8 Data analysis

The SICM data analysis was accomplished with XEI (Park system *Inc.* Santa, CA), Origin Pro (OriginLab Corp.) software, and Matlab (MathWorks). The 3D topography images were analyzed by XEI(Park Systems). Custom Matlab script was used to estimate the twitch force of the hECTs. Results are reported as mean ± SD. Gwyddion and ImageJ were used to assess the analysis of the of two-dimensional Fourier transform of the fluorescence images. To compare the data groups, one-way ANOVA-test and Mann Whitney-test were employed with $P \leq 0.05$ considered significantly different.

3. Results and Discussion

3.1 Electrical stimulation of the hECT

To deliver ES on cardiac tissues, direct coupling configuration is the most commonly used scheme. For this configuration, the pair of electrodes are in direct contact with the culture medium, which effectively delivers the electric field on the tissue. By applying a few volts of bias across the typical centimeter size tissue, the generated electric field on the tissue is approximately 3.3–5 V/cm[15, 31, 32], and the generated ionic current flow over the tissue can range from <5 mA to 65 mA[14, 33]. The tissue often can be electrically paced using this level of ES. However, the inconvenience of this method is related to the insufficient biocompatibility of the electrodes and the rising temperature that results in unwanted

physicochemical changes in the cell culture medium. We applied the ES in the capacitive coupling configuration to avoid these limitations and consider the added flexibility in system integration. Figure 1B (ii) shows that the two carbon plates are located outside the culture chamber and provide a uniform electric field to the hECT inserted between the two carbon plates. In our experiment, on the first day of beating, tissues were electrically stimulated using monophasic square wave pulses of 13 V/cm amplitude and 2 ms width at 5 Hz frequency. The 5 Hz ES frequency is chosen based on the fact that the rate of neonatal rat heart is about 4–8 Hz in the first three weeks after birth[34]. The 5 Hz frequency is also close to the value used in the previous electrical pacing study showing success in the development of t-tubule system in hECTs[31]. However, the hECTs in our experiments are observed not beating at the same ES frequency but rather at a slower rate. Therefore, the magnitude of the applied ES is below the excitation threshold to pace the hECT to beat at the applied rate.

The main drawback of this configuration is that a relatively high bias needs to be applied between the two electrodes to yield a comparable electric field across the tissue like that in the direct coupling configuration. Also, it is not straightforward to find the actual field magnitude applied in the medium. Therefore, we first used the finite element method (FEM) to simulate the static electric field in the culture medium (see Figure 2). When the applied external field is 13 V/cm, the simulated field in the solution is approximately 0.6 V/cm, which is reduced more than 20 times from the applied external field. We then directly measured the potential difference across the culture medium by using a high impedance differential amplifier. The measured mean electric field is approximately 0.55 V/cm, which is close to the simulated value (Figure 2D). We also measured the current density through the tissue culture medium during the ES (see supplementary information S2A). As shown in Figure 2E (black curve), the peak current magnitude in each pulse is approximately 1.5 mA/cm^2. This current is mainly derived from the charging current during the sudden change of the applied pulsatile bias. The steady current is close to zero in a pulse. For comparison, we measured the ionic current flow in the direct coupling configuration with an electric field of 13 V/cm (see the setup in Figure S2B). As shown in Figure 2E (red curve), the measured steady ionic current change in each pulse approximates a square wave shape. The steady ionic current density in the direct coupling configuration is also about 20 times higher in magnitude (about 30 mA/cm^2) than that of the peak current density in the capacitive coupling configuration. Therefore, the ES effect is mainly due to the electric field but not the ionic current flow in the capacitive coupling configuration.

3.2 Nanoscale topography images of the hECT

SICM has been successfully used to study the remodeling and alteration of t-tubules on the membranes of CMs isolated from matured heart tissues, which can provide more details than the typically used fluorescence imaging method with voltage sensitive dye di8-ANNEPs[20]. To make sure SICM can directly image the CMs on the surface of hECTs, we have conducted additional experiments to better understand the surface of the hECT. From the fluorescence images of the microsectioned hECT slices (about 10 μm thick) stained with Wheat Germ Agglutinin (WGA), we observed a continuous layer of cells at the surface of the hECT with highly branched t-tubule network (see Figure 3D and Figure S3). We also conducted whole cell patch-camp recordings by nanopipette on surface cells of live tissues

at randomly selected locations (see supplementary information Figure S4). We can acquire action potentials in most of the locations we probed, suggesting CMs are indeed on the surface of the hECTs.

Considering the structural heterogeneity of hECT, we have acquired SICM topography images of the fixed hECTs from three different regions: near the post, middle center and edge. Topography images from regions located at the edge of the hECT are shown in the left panel of Figure 3B. The hECTs without ES showed sparse features of Z-groove on the first 3 days of tissue culture. More structural changes of the cellular membrane in hECT began to be visible in the topography images on days 8 and 16, showing areas with valleys and crests. The valley and crest features are more evident in the height profile across the blue dash line at the top of each topography image. The valley is the opening of the t-tubules, and the domed crest is the region between the Z-grooves. The increased number of valley and crest features and their alignments reveal the development of the t-tubules system of the tissue. For comparison, the topography images of hECT with ES are shown in the right panel of Figure 3B. The domed crest between Z-grooves can already be resolved on day 3, and the better-aligned crests and z-grooves can be clearly identified on days 8 and 16. The height profile reveals that the spacing between Z-grooves was about 2 μm on day 16, close to the sarcomere length of adult ventricular CMs. This is because the transverse components of t-tubules regularly occur near sarcomeric zdiscs.

We have also investigated the development of the t-tubule structure near the edges of tissue in WGA stained thin hECT slices using fluorescence microscope. Figure 3D shows the fluorescence images of the transverse-sectioned slices and Figure S3 shows the cross-sectioned ones. On day 3, the t-tubule presented low density with short penetration length from the surface towards the axis of the hECT. In contrast, at the later days of culture (days 8 and 16), the t-tubule presented a network-like structure that penetrating deep from the surface. It is not easy to quantify the structural difference between tissues with and without ES. In general, we found the WGA intensity is higher across the whole slice of ES treated tissue, which implying a better developed t-tubule system. The t-tubule improvement revealed by SICM imaging and WGA fluorescence imaging results are consistent with the previous reports showing that electrical pacing can enhance t-tubulation[15, 31, 35].

Following the previous report, we calculated the Z-groove ratio[19]. The Z-groove ratio can better quantify the development of the t-tubule system, which is estimated by dividing the length of Z-grooves (indicated by the yellow dotted lines) by the total length of Z-groove if they were present on the whole surface (indicated by black dotted lines). The bigger z-groove ratio indicates the better development of the t-tubule system. For the adult ventricular CMs, the z-groove ratio is about 0.95[19, 20]. In Figure 3C, the Z-groove ratio of the hECT without ES is always lower than the value of hECT with ES on the same culture days from day 3 to 16. The significant differences were confirmed for tissues of days 5, 11 and 16 by an ANOVA test ($P < 0.05$). The increase of the Z-groove ratio is also clear for the hECT in the first week of ES. Our findings proved that electric field stimulation improved the t-tubulation and the remodeling of the membrane of the hECT towards a maturation stage.

Topography images at the surface region close to the post are shown in Figure 4A. The hECTs without ES began to show clear Z-groove at day 16, as indicated by the red dashed lines marked in the topography image. In contrast, obvious Z-grooves can be observed from day 3 of ES treated tissue. However, topography images of the hECT with ES only show sparse valleys and crest features. Topography images at the region close to the middle center of the hECTs are shown in Figure 4B. Even the Z-groove features were often absent and not clear in topography images for hECTs with or without ES. Therefore, the t-tubule network induced membrane remodeling is most developed for the CMs at the edges but least developed for the CMs in the middle of the hECT. Previous studies have shown that tension and stress are stronger at the edges and weaker in the middle of the suspended tissues[16, 36]. Therefore, the location-dependent membrane remodeling of the CMs in the hECT is explained by the different regional mechanical stress environment of the suspended hECT. In addition, in general, the membrane modeling of CM is always augmented by the effect of ES.

3.3 Sarcomere structural characterization of the hECT

The t-tubules system is closely related to the interior sarcomere structure. To confirm the development of t-tubule membrane structures, we also investigated the sarcomere organization of the interconnected hiPSC-CMs within the hECT. Figure 5A shows the representative immunofluorescence images of the hECT stained for α-actinin at different culture days. Sarcomere length was determined by measuring the distance between intensity peaks containing successive α-actinin striations. Figure 4B shows the measured sarcomere size change with the tissue culture time. For both hECTs with and without ES, the sarcomere size increases with the culture time. Without ES, the size increases from 1.54±0.22 μm at day 3 to1.79 ± 0.13 μm at day 16. With ES, the size of the sarcomere increases from 1.57±0.24 μm at day 3 to 1.89 ± 0.19 μm at day 16, which is close to the mature sarcomere length about 2.2 μm of adult ventricular CMs[37]. In addition, after 3–5 days in culture, the sarcomere elongated and aligned through the two PDMS posts. The ES impacted the sarcomere structure with better alignment and increased size at day 11 and 16 (additional images are included in supplementary information Figure S5). These results agree with previous studies that ES directs the hECTs towards a phenotype resembling adult-like myocardium[38].

3.4 Intracellular calcium imaging in the hECT

The t-tubules contain membrane microdomains enriched with ion channels and signaling molecules, such as L-type Ca^{2+} channel (LTCC) and Na^{+}/Ca^{2+} exchanger (NCX). Therefore, the t-tubules system directly relates to the calcium handling capability of the tissue. The better developed t-tubule system can synchronize the calcium release throughout the CMs in the hECT. In adult human cardiac tissue, calcium transients display a well-defined sequence of events initiated following each beat-to-beat action potential. We further explored the intracellular calcium transients within the hECT loaded with Fluo-4 to explore the dynamics of calcium handling. Three different regions were selected, and the increase in the concentration of calcium ions was represented as fluorescence intensity (F) of dye divided by the background intensity (F_0). The corresponding fluorescence images are shown in the supplementary information Figure S6A. Figure 6A shows the intracellular calcium

transients with an irregular shape and a higher frequency in the early maturation stage (day 2). In contrast, hECT under ES shows a homogenous shape and a slower beating frequency. Defined transients were visible in the later maturation stage at day 11 of culture. Figure 6B compares the shape of the representative calcium transients on the early and late maturation stages. The peak widths of calcium transients at day 2 are similar for the tissues with and without ES. In contrast, on day 11, the calcium transients are narrower for the tissue under ES. The full width also quantifies the peak width of the calcium transients at half maximum (FWHM). As shown in Figure 5C, between the tissues with and without ES, the FWHM has no significant difference at the early stage. However, the hECTs with ES show an evident decrease in FWHM at the late stage, suggesting an improvement in intracellular calcium kinetics. In addition, the decay time of the calcium transients for the hECTs with ES is significantly reduced at day 11 (see supplementary information Figure S6B). This result suggests a fast removal of intracellular calcium for the day 11 tissues with ES. This condition may be generated by enhancing the expression of SERCA pump and Na/Ca exchanger (NCX). It should be noted that the calcium transients collected at day 11 often showed a clear downward peak right after the upstroke, which is generated by the contraction motion of the hECT at the time of fluorescence imaging data collection. This tissue motion-induced artifact in fluorescence intensity change is often not evident at day 2 because the contraction motion is weaker at the early stage.

3.5 Twitch force and beating frequency.

Transduction of the electrical signal results in oscillations of the intracellular calcium concentration, which permits the interaction between the myosin and actin molecules and the ATP hydrolysis. Due to the synchronized calcium release, the better developed t-tubule system allows the interconnected CMs in the hECT to contract more forcefully. We also measured the force contraction and beating frequency of the hECT with and without ES after 4, 7, 9, and 11 days of culture. Figure 6A shows typical recordings of the force contraction time traces without and with ES. Small fluctuations in peak magnitude between each contraction are often noticed for hECT at day 4 without ES, attributed to the partial electromechanical coupling of the CMs in hECT at the early maturation stage. Figure 6B compares the force peak shape. The peak width is generally bigger for the hECT with ES on day 11. The broader peak suggests the contraction lasts longer for the hECT with ES. The twitch force peak magnitude and the beating rate as a function of culture time are shown in Figure 6C. The twitch force magnitude for both tissues increases with the culture time, suggesting the maturation of the tissue. From days 7 to 11, the hECTs with ES generate a considerably higher twitch force. Statistical significant differences are observed for the twitch force of tissues on days 7 and 11 (see Figure 7D). Meanwhile, the tissues with ES show a reduced beating rate (see the bottom panels of Figures 7C and 7D). It should be noted that the beating rate here is smaller than the results in Figure 7, which is attributed to the temperature effect (see supplementary information Figure S7). We also notice that the force does not increase monotonically and is slightly reduced from day 7 to 9 for hECTs either with or without ES. This is attributed to hECT reorganization, as discussed below. These findings are consistent with the observed development of the t-tubule system. They can be explained by the improved calcium handling, where the force and frequency contraction depends on the balance between calcium influx, sarcoplasmic storage,

and release[4, 39]. Also, our results may be related to the possible switching in the relative expression from the faster α isoform of the myosin heavy chain expressed in neonatal CMs to the slower β isoform of the myosin heavy chain that is expressed in mature CMs[40].

3.6 Geometrical changes of hECTs with and without ES

The hECTs in the milli-tug formation also underwent noticeable geometrical changes at the macro scale. We noticed that the volume of the hECT often became bigger during culture without ES but always became smaller with ES. Because the change of hECT thickness is relatively small, we quantify the observed volume change by change of the cross-section width of the tissue (see Figure S8). The tissues without ES showed a continued increase in the cross-section width from 731 ± 82 μm to 776 ± 60 μm. In contrast, tissues under ES showed a decrease of the cross-section width from 667 ± 61 μm to 614 ± 63 μm. These different geometrical changes for tissues with and without ES may reflect the ES induced different cell composition, morphology and size changes as well as more dynamic reorganization processes of the tissue. In the optical images, the edges of the hECTs (both with and without ES) at day 11 appear rougher with ‘bead’ like strucures, which maybe attributed to the cells been squeezed out of the matrix due to the structural reorganization. We have observed the relatively higher nuclei/sarcomere volume ratio for the hECTs without ES at the later day (day 11) by using the z-stacks of the immunofluorescence confocal images (see supplementary information Figure S9). We have also isolated some cells from the day 16 tissue using papain enzyme (see section S8 of supporting information)[15]. The cells from tissue without ES show large variations in size and shape. In contrast, the shape of cells from tissue with ES is more uniform in the elongated shape (see Figure S10).

We have also carried out noninvasive indentation experiments to probe the overall mechanical properties of the suspended live hECTs in the milli-tug formation (see section S11 of supporting information). The stiffness of tissue with ES treatment is higher in average. However, due to the large variations, the conclusion of mechanical test is not conclusive.

4. Conclusion

In summary, we have studied the effect of continuous subthreshold ES in the capacitive coupling configuration on the development of hECTs in 3D constructs prepared in a milli-tug device. We monitored the structural and functional changes of the millimeter size hECTs over two weeks of culture time with ES. Along with the conventional methods, including immunofluorescence imaging of sarcomere structure, WGA staining for t-tubule network development, fluorescence imaging of calcium handling, and twitch force measurements, we also applied SICM to characterize the maturation process of hECTs. The SICM topography images showed the fine and detailed membrane structural changes and revealed the development of the t-tubules system.With the ES, the regular crest/valley patterns with a spatial period close to 2 μm appeared on the cellular surface of hiPSC-CMs at the edges of hECTs, demonstrating better development of the t-tubule network. The better-developed membrane structures of the t-tubule system are consistent with the sarcomere structure development, enabling effective electrical signal propagation as revealed by the calcium

handling measurements. Accordingly, the hECT under ES generates a more prominent twitch force with a reduced beating frequency. However, the degree of maturity of hECTs under ES reported here is not enough to fully recapitulate the structural and functional properties seen in adult myocardium and further optimization of the method is needed. For the subthreshold ES we applied here, the hECTs are not forced to beat at the rate of the stimulation frequency. Therefore, the contribution from the intense physical training during electrical pacing is small. As previously reported, the ES on non-excitable cells can increase the activity of ion channels and trigger a variety of intracellular signaling pathways and affect various cellular responses, including migration, alignment, proliferation, and differentiation[41]. The ES might also trigger the expression of mechanoreceptors (mediation of force transmission) and improve calcium handling[42]. The work suggests that the long-term subthreshold ES in the capacitive coupling configuration can still have a positive effect on the maturation of hECTs formed from early-stage hiPSC-CMs. In addition, the SICM can be useful to monitor the ultrastructural development during the maturation process of hECTs.

Supplementary Material

Refer to Web version on PubMed Central for supplementary material.

Acknowledgment

We acknowledge the share of protocols for culturing hiPSC cells and forming the hECT on milli-tug from Chris Chen's lab, the share of electrical stimulation method from Godana Dukovic's lab, and the share of the twitch force measurement method by Thomas Bifano's lab. This work was mainly supported by the ERC program of NSF under NSF Cooperative Agreement No. EEC-1647837. The SICM work was also partially supported by NSF (CBET1454544) to J.H. P.P acknowledge the support from FIU CASE for providing postdoctoral fellowship. We also acknowledge using machines and electronic shops of FIU CASE.

Data availability

All the relevant data are available with the article and the Supplementary information files, or available from the corresponding author upon reasonable request.

References

(1). Bergmann O; Bhardwaj RD; Bernard S; Zdunek S; Barnabé-Heider F; Walsh S; Zupicich J; Alkass K; Buchholz BA; Druid H; et al. Evidence for Cardiomyocyte Renewal in Humans. Science 2009, 324 (5923), 98. DOI: 10.1126/science.1164680. [PubMed: 19342590] Derks W; Murganti F; Bergmann O Cardiomyocyte renewal in the failing heart: lessons from the neonate? Biophysical Reviews 2020, 12 (4), 785–787. DOI: 10.1007/s12551-020-00739-9. [PubMed: 32681468]

(2). Bedada Fikru B.; Chan Sunny S.-K.; Metzger Stefania K.; Zhang L; Zhang J; Garry Daniel J.; Kamp Timothy J.; Kyba M; Metzger Joseph M. Acquisition of a Quantitative, Stoichiometrically Conserved Ratiometric Marker of Maturation Status in Stem Cell-Derived Cardiac Myocytes. Stem Cell Reports 2014, 3 (4), 594–605. DOI: 10.1016/j.stemcr.2014.07.012. [PubMed: 25358788] Koivumäki JT; Naumenko N; Tuomainen T; Takalo J; Oksanen M; Puttonen KA; Lehtonen Š; Kuusisto J; Laakso M; Koistinaho J; et al. Structural Immaturity of Human iPSC-Derived Cardiomyocytes: In Silico Investigation of Effects on Function and Disease Modeling. Frontiers in Physiology 2018, 9, 80, 10.3389/fphys.2018.00080.Poon E; Kong C.-w.; Li RA Human Pluripotent Stem Cell-Based Approaches for Myocardial Repair: From

the Electrophysiological Perspective. Molecular Pharmaceutics 2011, 8 (5), 1495–1504. DOI: 10.1021/mp2002363. [PubMed: 21879736]

(3). Guo Y; Pu William T Cardiomyocyte Maturation. Circulation Research 2020, 126 (8), 1086–1106. DOI: 10.1161/CIRCRESAHA.119.315862 (acccessed 2020/11/20). [PubMed: 32271675] Machiraju P; Greenway SC Current methods for the maturation of induced pluripotent stem cell-derived cardiomyocytes. World J Stem Cells 2019, 11 (1), 33–43. DOI: 10.4252/wjsc.v11.i1.33 [PubMed: 30705713]

(4). Lundy SD; Zhu W-Z; Regnier M; Laflamme MA Structural and Functional Maturation of Cardiomyocytes Derived from Human Pluripotent Stem Cells. Stem Cells and Development 2013, 22 (14), 1991–2002. DOI: 10.1089/scd.2012.0490 (acccessed 2021/03/20). [PubMed: 23461462]

(5). Lewandowski J; Rozwadowska N; Kolanowski TJ; Malcher A; Zimna A; Rugowska A; Fiedorowicz K; Łabędź W; Kubaszewski Ł; Chojnacka K; et al. The impact of in vitro cell culture duration on the maturation of human cardiomyocytes derived from induced pluripotent stem cells of myogenic origin. Cell Transplantation 2018, 27 (7), 1047–1067. DOI: 10.1177/0963689718779346 (acccessed 2022/04/18). [PubMed: 29947252]

(6). Ribeiro Alexandre JS; Ang Y-S; Fu J-D; Rivas Renee N; Mohamed Tamer MA; Higgs Gadryn C; Srivastava D; Pruitt Beth L Contractility of single cardiomyocytes differentiated from pluripotent stem cells depends on physiological shape and substrate stiffness. Proceedings of the National Academy of Sciences 2015, 112 (41), 12705–12710. DOI: 10.1073/pnas.1508073112 (acccessed 2022/04/18).

(7). Navaei A; Saini H; Christenson W; Sullivan RT; Ros R; Nikkhah M Gold nanorod-incorporated gelatin-based conductive hydrogels for engineering cardiac tissue constructs. Acta Biomaterialia 2016, 41, 133–146. DOI: 10.1016/j.actbio.2016.05.027. [PubMed: 27212425] Saleh TM; Ahmed EA; Yu L; Kwak H-H; Hussein KH; Park K-M; Kang B-J; Choi K-Y; Kang K-S; Woo H-M Incorporation of nanoparticles into transplantable decellularized matrices: Applications and challenges. The International Journal of Artificial Organs 2018, 41 (8), 421–430. DOI: 10.1177/0391398818775522 (acccessed 2022/04/18). [PubMed: 29807488]

(8). Jackman CP; Carlson AL; Bursac N Dynamic culture yields engineered myocardium with nearadult functional output. Biomaterials 2016, 111, 66–79. DOI: 10.1016/j.biomaterials.2016.09.024. [PubMed: 27723557]

(9). Yoshida S; Miyagawa S; Fukushima S; Kawamura T; Kashiyama N; Ohashi F; Toyofuku T; Toda K; Sawa Y Maturation of Human Induced Pluripotent Stem Cell-Derived Cardiomyocytes by Soluble Factors from Human Mesenchymal Stem Cells. Molecular Therapy 2018, 26 (11), 2681–2695. DOI: 10.1016/j.ymthe.2018.08.012. [PubMed: 30217728] Feyen DAM; McKeithan WL; Bruyneel AAN; Spiering S; Hörmann L; Ulmer B.; Zhang H; Briganti F; Schweizer M; Hegyi B; et al. Metabolic Maturation Media Improve Physiological Function of Human iPSC-Derived Cardiomyocytes. Cell Reports 2020, 32 (3), 107925. DOI: 10.1016/j.celrep.2020.107925. [PubMed: 32697997]

(10). Ruan J-L; Tulloch NL; Razumova MV; Saiget M; Muskheli V; Pabon L; Reinecke H; Regnier M; Murry CE Mechanical Stress Conditioning and Electrical Stimulation Promote Contractility and Force Maturation of Induced Pluripotent Stem Cell-Derived Human Cardiac Tissue. Circulation 2016, 134 (20), 1557–1567. DOI: 10.1161/CIRCULATIONAHA.114.014998 [PubMed: 27737958]

(11). Ronaldson-Bouchard K; Yeager K; Teles D; Chen T; Ma S; Song L; Morikawa K; Wobma HM; Vasciaveo A; Ruiz EC; et al. Engineering of human cardiac muscle electromechanically matured to an adult-like phenotype. Nature Protocols 2019, 14 (10), 2781–2817. DOI: 10.1038/s41596-019-0189-8. [PubMed: 31492957] Boudou T; Legant WR; Mu A; Borochin MA; Thavandiran N; Radisic M; Zandstra PW; Epstein JA; Margulies KB; Chen CSA microfabricated platform to measure and manipulate the mechanics of engineered cardiac microtissues. Tissue Eng Part A 2012, 18 (9–10), 910–919. DOI: 10.1089/ten.tea.2011.0341 [PubMed: 22092279] Miller KL; Xiang Y; Yu C; Pustelnik J; Wu J; Ma X; Matsui T; Imahashi K; Chen S Rapid 3D BioPrinting of a human iPSC-derived cardiac micro-tissue for highthroughput drug testing. Organs-on-a-Chip 2021, 3, 100007. DOI: 10.1016/j.ooc.2021.100007.

(12). Zimmermann WH; Schneiderbanger K; Schubert P; Didié M; Münzel F; Heubach JF; Kostin S; Neuhuber WL; Eschenhagen T Tissue Engineering of a Differentiated Cardiac Muscle

Construct. Circulation Research 2002, 90 (2), 223–230. DOI: 10.1161/hh0202.103644 (acccessed 2020/11/16). [PubMed: 11834716] Visone R; Talò G; Occhetta P; Cruz-Moreira D; Lopa S; Pappalardo OA; Redaelli A; Moretti M; Rasponi M A microscale biomimetic platform for generation and electro-mechanical stimulation of 3D cardiac microtissues. APL Bioengineering 2018, 2 (4), 046102. DOI: 10.1063/1.5037968 (acccessed 2020/11/21). [PubMed: 31069324]

(13). Nunes SS; Miklas JW; Liu J; Aschar-Sobbi R; Xiao Y; Zhang B; Jiang J; Massé S; Gagliardi M; Hsieh A; et al. Biowire: a platform for maturation of human pluripotent stem cell–derived cardiomyocytes. Nature Methods 2013, 10 (8), 781–787. DOI: 10.1038/nmeth.2524. [PubMed: 23793239]

(14). Hirt MN; Boeddinghaus J; Mitchell A; Schaaf S; Börnchen C; Müller C; Schulz H; Hubner N; Stenzig J; Stoehr A; et al. Functional improvement and maturation of rat and human engineered heart tissue by chronic electrical stimulation. Journal of Molecular and Cellular Cardiology 2014, 74, 151–161. DOI: [PubMed: 24852842]

(15). Ronaldson-Bouchard K; Ma SP; Yeager K; Chen T; Song L; Sirabella D; Morikawa K; Teles D; Yazawa M; Vunjak-Novakovic G Advanced maturation of human cardiac tissue grown from pluripotent stem cells. Nature 2018, 556 (7700), 239–243. DOI: 10.1038/s41586-018-0016-3. [PubMed: 29618819]

(16). Fink C; Ergün S; Kralisch D; Remmers U; Weil J; Eschenhagen T Chronic stretch of engineered heart tissue induces hypertrophy and functional improvement. The FASEB Journal 2000, 14 (5), 669–679, https://doi.org/10.1096/fasebj.14.5.669. DOI: 10.1096/fasebj.14.5.669 (acccessed 2020/11/16). [PubMed: 10744624]

(17). Thrivikraman G; Boda SK; Basu B Unraveling the mechanistic effects of electric field stimulation towards directing stem cell fate and function: A tissue engineering perspective. Biomaterials 2018, 150, 60–86. DOI: 10.1016/j.biomaterials.2017.10.003. [PubMed: 29032331] Hiemer B; Krogull M; Bender T; Ziebart J; Krueger S; Bader R; Jonitz-Heincke A Effect of electric stimulation on human chondrocytes and mesenchymal stem cells under normoxia and hypoxia. Mol Med Rep 2018, 18 (2), 2133–2141. DOI: 10.3892/mmr.2018.9174. [PubMed: 29916541]

(18). Hansma P; Drake B; Marti O; Gould S; Prater C The scanning ion-conductance microscope. Science 1989, 243 (4891), 641– 643. [PubMed: 2464851] Korchev Y; Bashford C; Milovanovic M; Vodyanoy I; Lab M Scanning ion conductance microscopy of living cells. Biophys J 1997, 73 (2), 653– 658. [PubMed: 9251784] Miragoli M; Moshkov A; Novak P; Shevchuk A; Nikolaev VO; El-Hamamsy I; Potter CMF; Wright P; Kadir SHSA; Lyon AR; et al. Scanning ion conductance microscopy: a convergent high-resolution technology for multi-parametric analysis of living cardiovascular cells. Journal of the Royal Society, Interface 2011, 8, 913–925, Journal Article. DOI: 10.1098/rsif.2010.0597. [PubMed: 21325316] Chen CC; Zhou Y; Baker LA Scanning ion conductance microscopy. Annual review of analytical chemistry 2012, 5, 207–228. DOI: 10.1146/annurev-anchem-062011-143203.

(19). Gorelik J; Yang LQ; Zhang Y; Lab M; Korchev Y; Harding SE A novel Z-groove index characterizing myocardial surface structure. Cardiovascular Research 2006, 72 (3), 422–429. DOI: 10.1016/j.cardiores.2006.09.009 (acccessed 3/7/2021). [PubMed: 17054929]

(20). Lyon AR; MacLeod KT; Zhang Y; Garcia E; Kanda GK; Lab MJ; Korchev YE; Harding SE; Gorelik J Loss of T-tubules and other changes to surface topography in ventricular myocytes from failing human and rat heart. Proc Natl Acad Sci U S A 2009, 106 (16), 6854–6859. DOI: 10.1073/pnas.0809777106 [PubMed: 19342485]

(21). Park SH; Kim A; An J; Cho HS; Kang TM Nanoscale imaging of rat atrial myocytes by scanning ion conductance microscopy reveals heterogeneity of T-tubule openings and ultrastructure of the cell membrane. The Korean journal of physiology & pharmacology : official journal of the Korean Physiological Society and the Korean Society of Pharmacology 2020, 24 (6), 529–543. DOI: 10.4196/kjpp.2020.24.6.529 From NLM. [PubMed: 33093274]

(22). Hong T; Shaw RM Cardiac T-Tubule Microanatomy and Function. Physiological reviews 2017, 97 (1), 227–252. DOI: 10.1152/physrev.00037.2015 [PubMed: 27881552]

(23). Lian X; Hsiao C; Wilson G; Zhu K; Hazeltine LB; Azarin SM; Raval KK; Zhang J; Kamp TJ; Palecek SP Robust cardiomyocyte differentiation from human pluripotent stem cells via temporal

modulation of canonical Wnt signaling. Proceedings of the National Academy of Sciences 2012, 109 (27), E1848. DOI: 10.1073/pnas.1200250109.

(24). Tohyama S; Hattori F; Sano M; Hishiki T; Nagahata Y; Matsuura T; Hashimoto H; Suzuki T; Yamashita H; Satoh Y; et al. Distinct Metabolic Flow Enables Large-Scale Purification of Mouse and Human Pluripotent Stem Cell-Derived Cardiomyocytes. Cell Stem Cell 2013, 12 (1), 127–137. DOI: 10.1016/j.stem.2012.09.013. [PubMed: 23168164]

(25). Legant WR; Pathak A; Yang MT; Deshpande VS; McMeeking RM; Chen CS Microfabricated tissue gauges to measure and manipulate forces from 3D microtissues. Proceedings of the National Academy of Sciences 2009, 106 (25), 10097. DOI: 10.1073/pnas.0900174106.

(26). Kaiser NJ; Kant RJ; Minor AJ; Coulombe KLK Optimizing Blended Collagen-Fibrin Hydrogels for Cardiac Tissue Engineering with Human iPSC-derived Cardiomyocytes. ACS Biomaterials Science & Engineering 2019, 5 (2), 887–899. DOI: 10.1021/acsbiomaterials.8b01112. [PubMed: 30775432]

(27). Sniadecki NJ; Chen CS Microfabricated Silicone Elastomeric Post Arrays for Measuring Traction Forces of Adherent Cells. In Methods in Cell Biology, Vol. 83; Academic Press, 2007; pp 313–328. [PubMed: 17613314]

(28). Chen F; Manandhar P; Ahmed MS; Chang S; Panday N; Zhang H; Moon JH; He J Extracellular Surface Potential Mapping by Scanning Ion Conductance Microscopy Revealed Transient Transmembrane Pore Formation Induced by Conjugated Polymer Nanoparticles. Macromolecular Bioscience 2019, 19 (2), 1800271. DOI: 10.1002/mabi.201800271 (acccessed 2019/09/22).

(29). Jung GE; Noh H; Shin YK; Kahng SJ; Baik KY; Kim HB; Cho NJ; Cho SJ Closed-loop ARS mode for scanning ion conductance microscopy with improved speed and stability for live cell imaging applications. Nanoscale 2015, 7 (25), 10989–10997. DOI: 10.1039/c5nr01577d From NLM. [PubMed: 25959131]

(30). Novak P; Li C; Shevchuk AI; Stepanyan R; Caldwell M; Hughes S; Smart TG; Gorelik J; Ostanin VP; Lab MJ; et al. Nanoscale live-cell imaging using hopping probe ion conductance microscopy. Nat Methods 2009, 6 (4), 279–281. DOI: 10.1038/nmeth.1306. [PubMed: 19252505]

(31). Godier-Furnémont AFG; Tiburcy M; Wagner E; Dewenter M; Lämmle S; El-Armouche A; Lehnart SE; Vunjak-Novakovic G; Zimmermann W-H Physiologic force-frequency response in engineered heart muscle by electromechanical stimulation. Biomaterials 2015, 60, 82–91. DOI: 10.1016/j.biomaterials.2015.03.055. [PubMed: 25985155]

(32). Zhao Y; Rafatian N; Feric NT; Cox BJ; Aschar-Sobbi R; Wang EY; Aggarwal P; Zhang B; Conant G; Ronaldson-Bouchard K; et al. A Platform for Generation of Chamber-Specific Cardiac Tissues and Disease Modeling. Cell 2019, 176 (4), 913–927.e918. DOI: 10.1016/j.cell.2018.11.042. [PubMed: 30686581]

(33). McDonough PM; Glembotski CC Induction of atrial natriuretic factor and myosin light chain-2 gene expression in cultured ventricular myocytes by electrical stimulation of contraction. Journal of Biological Chemistry 1992, 267 (17), 11665–11668. DOI: 10.1016/S0021-9258(19)49744-5. [PubMed: 1376309]

(34). Malfatto G; Rosen TS; Steinberg SF; Ursell PC; Sun LS; Daniel S; Danilo P; Rosen MR Sympathetic neural modulation of cardiac impulse initiation and repolarization in the newborn rat. Circulation Research 1990, 66 (2), 427–437. DOI: 10.1161/01.RES.66.2.427 (acccessed 2022/04/18). [PubMed: 2153471] Vornanen M Force-frequency relationship, contraction duration and recirculating fraction of calcium in postnatally developing rat heart ventricles: correlation with heart rate. Acta Physiologica Scandinavica 1992, 145 (4), 311–321, https://doi.org/10.1111/j.1748–1716.1992.tb09371.x. DOI: 10.1111/j.1748-1716.1992.tb09371.x (acccessed 2022/04/18). [PubMed: 1529721]

(35). Radisic M; Park H; Shing H; Consi T; Schoen FJ; Langer R; Freed LE; Vunjak-Novakovic G Functional assembly of engineered myocardium by electrical stimulation of cardiac myocytes cultured on scaffolds. Proceedings of the National Academy of Sciences 2004, 101 (52), 18129. DOI: 10.1073/pnas.0407817101.

(36). Sander EA; Barocas VH; Tranquillo RT Initial Fiber Alignment Pattern Alters Extracellular Matrix Synthesis in Fibroblast-Populated Fibrin Gel Cruciforms and Correlates with Predicted Tension. Annals of Biomedical Engineering 2011, 39 (2), 714–729. DOI: 10.1007/

s10439-010-0192-2. [PubMed: 21046467] Bose P; Eyckmans J; Nguyen TD; Chen CS; Reich, DH Effects of Geometry on the Mechanics and Alignment of Three-Dimensional Engineered Microtissues. ACS Biomaterials Science & Engineering 2019, 5 (8), 3843–3855. DOI: 10.1021/acsbiomaterials.8b01183. [PubMed: 33438424]

(37). Karbassi E; Fenix A; Marchiano S; Muraoka N; Nakamura K; Yang X; Murry CE Cardiomyocyte maturation: advances in knowledge and implications for regenerative medicine. Nature Reviews Cardiology 2020, 17 (6), 341–359. DOI: 10.1038/s41569-019-0331-x. [PubMed: 32015528]

(38). Lasher RA; Pahnke AQ; Johnson JM; Sachse FB; Hitchcock RW Electrical stimulation directs engineered cardiac tissue to an age-matched native phenotype. J Tissue Eng 2012, 3 (1), 2041731412455354-2041731412455354. DOI: 10.1177/2041731412455354Tandon N; Cannizzaro C; Chao P-HG; Maidhof R; Marsano A; Au HTH; Radisic M; Vunjak-Novakovic G Electrical stimulation systems for cardiac tissue engineering. Nature Protocols 2009, 4 (2), 155–173. DOI: 10.1038/nprot.2008.183. [PubMed: 19180087]

(39). Sasaki D; Matsuura K; Seta H; Haraguchi Y; Okano T; Shimizu T Contractile force measurement of human induced pluripotent stem cell-derived cardiac cell sheet-tissue. PLOS ONE 2018, 13 (5), e0198026. DOI: 10.1371/journal.pone.0198026. [PubMed: 29791489]

(40). Lompré A-M; Mercadier J-J; Schwartz K Changes in Gene Expression during Cardiac Growth. In International Review of Cytology, Jeon KW, Friedlander M Eds.; Vol. 124; Academic Press, 1991; pp 137–186. [PubMed: 1825818] Schwan J; Campbell SG Article Commentary: Prospects for In Vitro Myofilament Maturation in Stem Cell-Derived Cardiac Myocytes: Supplementary Issue: Stem Cell Biology. Biomark Insights 2015, 10s1, BMI.S23912. DOI: 10.4137/BMI.S23912 (acccessed 2021/03/21).

(41). Love MR; Palee S; Chattipakorn SC; Chattipakorn N Effects of electrical stimulation on cell proliferation and apoptosis. Journal of Cellular Physiology 2018, 233 (3), 1860–1876, https://doi.org/10.1002/jcp.25975. DOI: 10.1002/jcp.25975 (acccessed 2021/05/01). [PubMed: 28452188] Balint R; Cassidy NJ; Cartmell SH Electrical Stimulation: A Novel Tool for Tissue Engineering. Tissue Engineering Part B: Reviews 2012, 19 (1), 48–57. DOI: 10.1089/ten.teb.2012.0183 (acccessed 2021/05/01). [PubMed: 22873689] Krueger S; Riess A; Jonitz-Heincke A; Weizel A; Seyfarth A; Seitz H; Bader R Establishment of a New Device for Electrical Stimulation of Non-Degenerative Cartilage Cells In Vitro. International Journal of Molecular Sciences 2021, 22 (1). DOI: 10.3390/ijms22010394.

(42). Echenique AM; Graffigna JP Electrical stimulation of mechanoreceptors. Journal of Physics: Conference Series 2011, 332, 012044. DOI: 10.1088/1742-6596/332/1/012044.

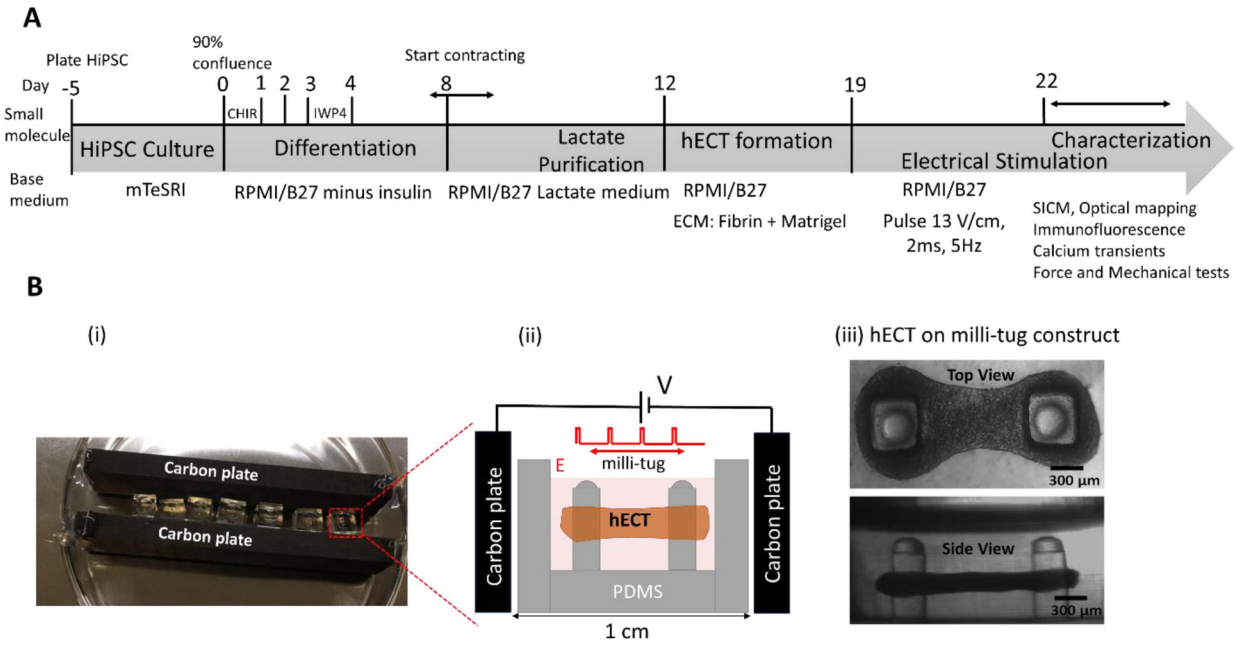

Figure 1.

(A) Timeline for the formation of hiPSC-CMs derived hECT and the following characterizations. (B) (i) The photo image of the ES setup. (ii) The diagram illustrates the capacitive coupling configuration and the hECT in the milli-tug construct. (iii) The transmitted-light optical microscope images (both top and side views) of a live hECT in the milli-tug construct. Tissues were placed under ES on the first day of spontaneous beating.

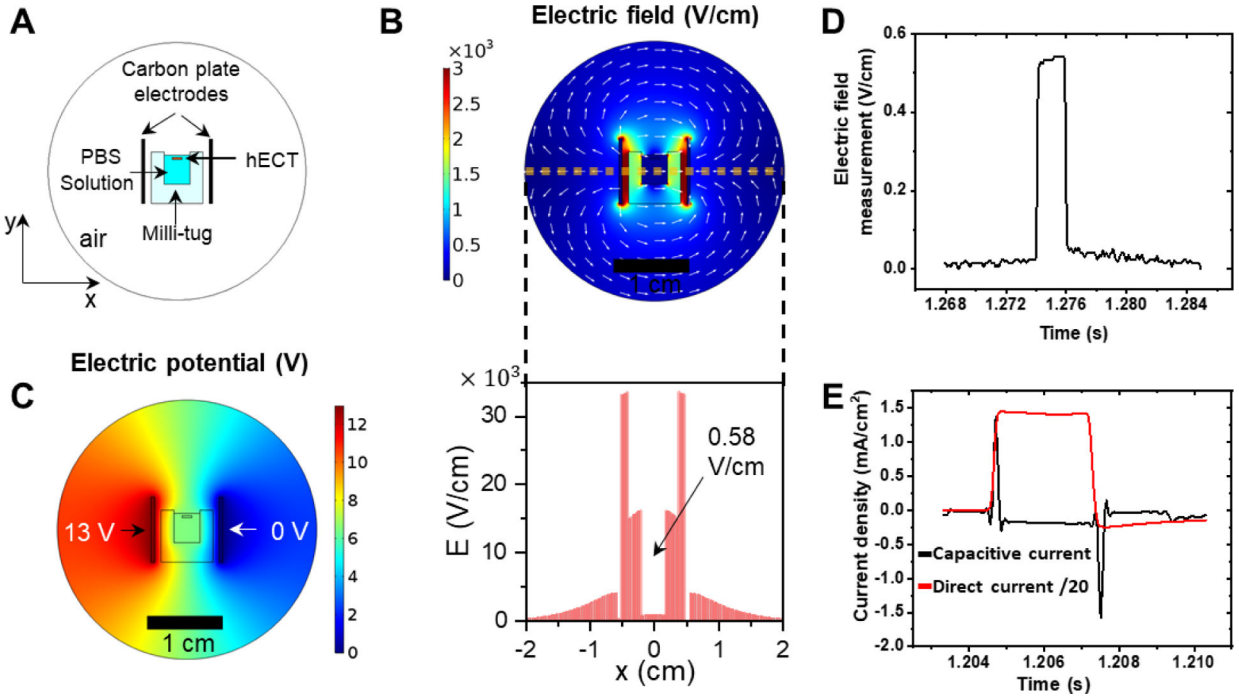

Figure 2.

Characterization of the electrical stimulation. (A) Snapshot of 2D stationary FEM model used for simulation. Two carbon plate electrodes were placed 1 cm apart, and 13V potential was applied between them. The figures are drawn to scale. (B) The electric field distribution between two carbon plate electrodes. The white arrows indicate the direction of the field, and the color bar shows the intensity of the field. The distribution of the total electric field along the yellow dash line is shown below. The E field in the PBS bath (indicated by the black arrow) is estimated to be ~0.58 V/cm. (C) The distribution of potential between carbon plate electrodes. (D) Experimental measurement of the electric field with a magnitude of 0.55 V/cm in the milli-tug. (E) Current density through the culture medium in direct and capacitive coupling configuration during stimulation. For better comparison, the current density in direct current configuration was reduced 20 times.

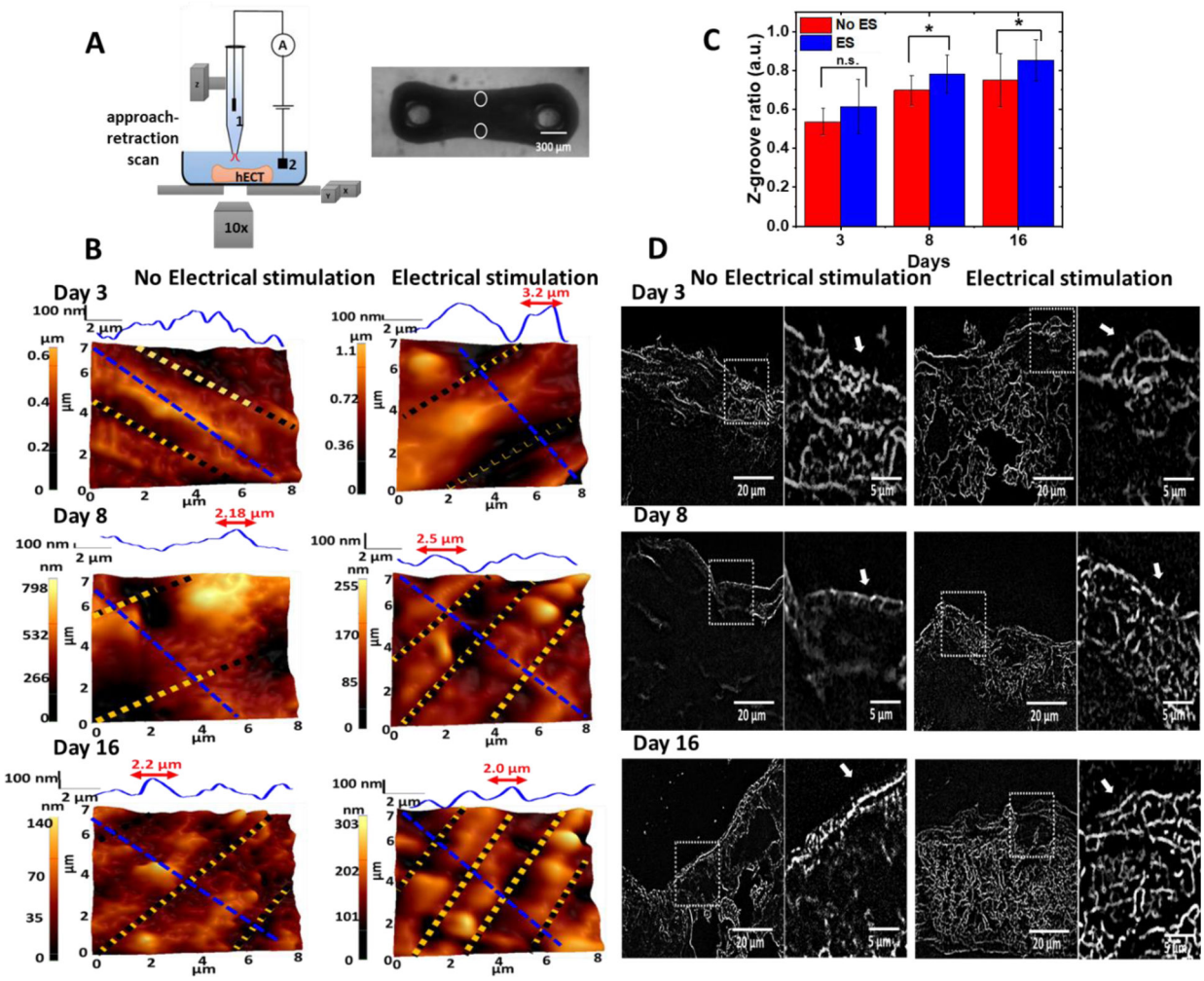

Figure 3. SICM topography images of the hECTs.

(A) Illustration of the SICM setup on acquiring the topography images from the edges of the hECT indicated by the white circles in the optical image of the hECT. The nanopipette is mounted on a Z-piezo actuator. The ion current that flows through the Ag/AgCl electrodes 1 and 2 is used as the feedback signal to control the distance between the nanopipette tip and the tissue membrane. (B) Topography images of the membrane surface on the edges of the hECTs at different culture days without and with ES. Height profiles are through the blue dashed lines marked in the topography images. Z-grooves are indicated by the yellow and black dotted lines that are used to estimate the Z-groove ratio. (C) Statistical analysis of the Z-groove ratio for the hECTs without and with ES. The ANOVA test confirmed significant differences in the Z-groove ratio (N=3,with 4–5 repeats). (D) Representative transversesectioned slices stained with WGA in hECTs at different culture time with and without ES. White arrows in the zoom-in images indicate the formation of the t-tubule network.

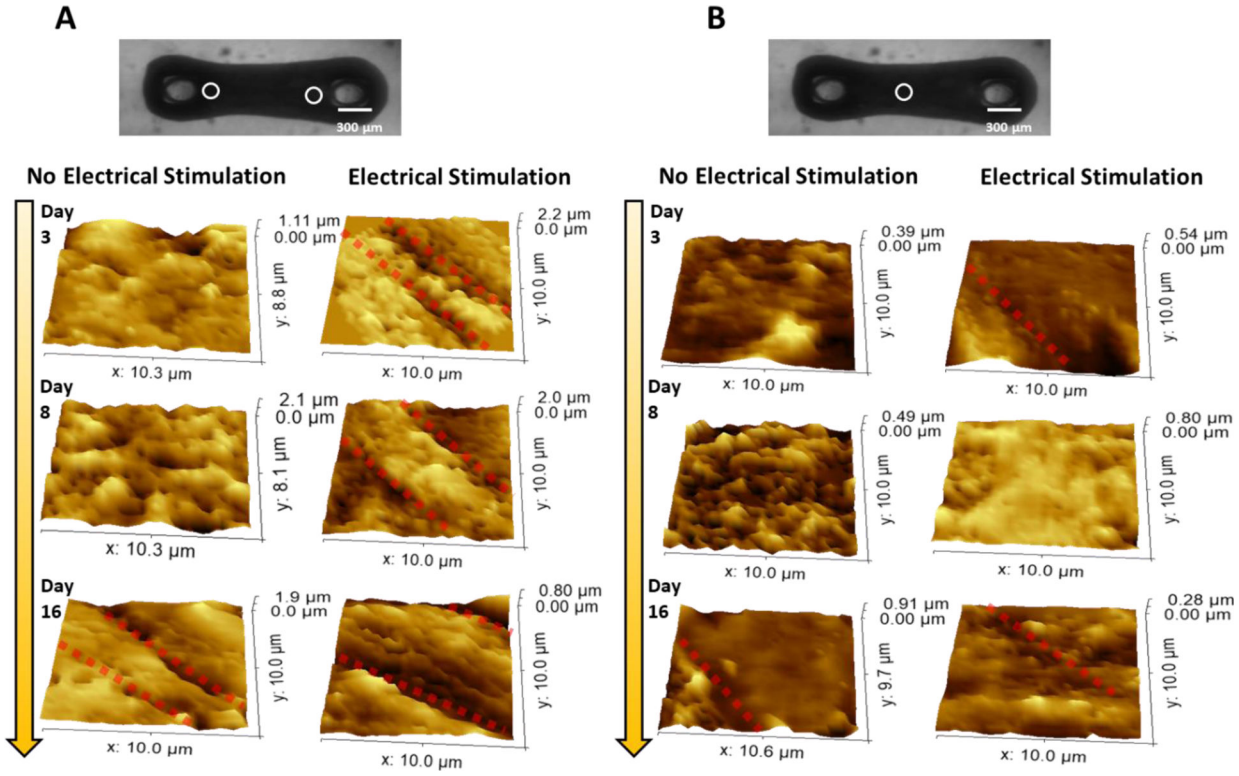

Figure 4. SICM topography images of regions close to the post and middle center of the hECT.

(A, B) Topography images of the regions close to the post (A) and middle center (B) of the hECT without and with ES at different culture days. The location of scanning is indicated by the white circles in the optical image of a hECT. The clear Z-groove features are indicated by red-dotted lines in the topography images.

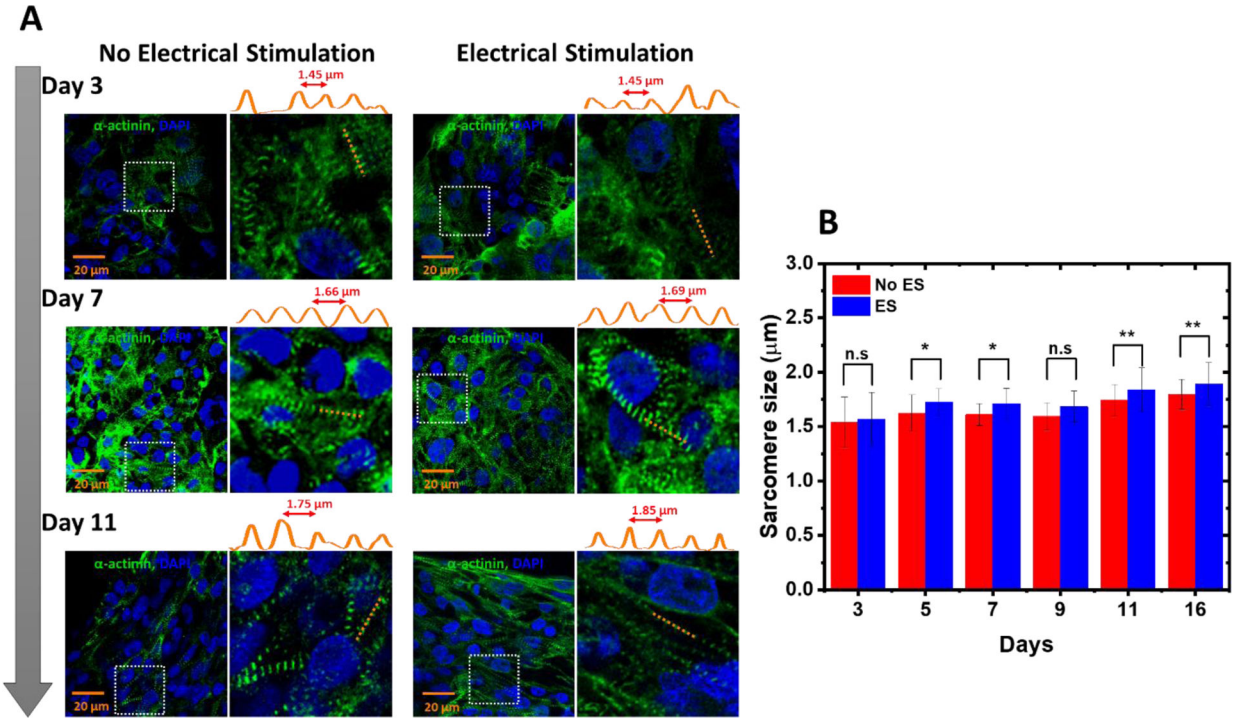

Figure 5. Effects of ES on the hECT sarcomere structure.

(A) Representative immunostained images of the structural organization in the hECT stained for α-actinin (green) and nucleus (blue). The intensity profiles along the orange dashed lines are shown on top of each fluorescence image. (B) Statistical analysis of the sarcomere size for the hECT without and with ES (N=20, from two samples per day and three repeats of each sample). The ANOVA test confirmed significant differences in the sarcomere size.

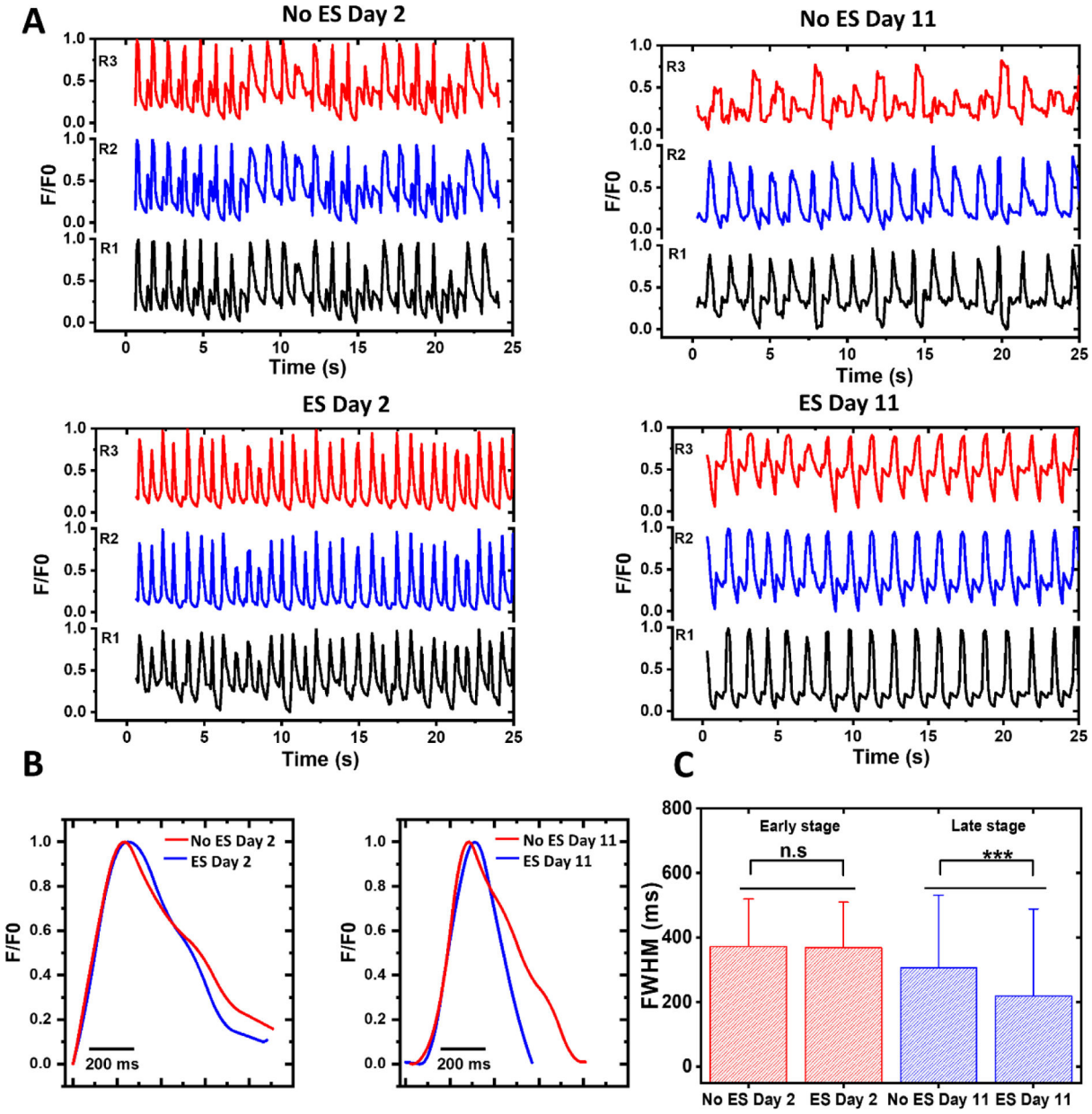

Figure 6. Calcium transients in the hECT.

(A) Recordings of calcium transients without and with ES at three different regions in the hECTs at day 2 (left) and 11 (right). (B) Representative calcium transients on early (day 2) and late maturation stages (day 11). (C) The FWHM of the calcium transients at the early and late stages (from two samples per day and three repeats per sample). The error bar is the standard deviation.

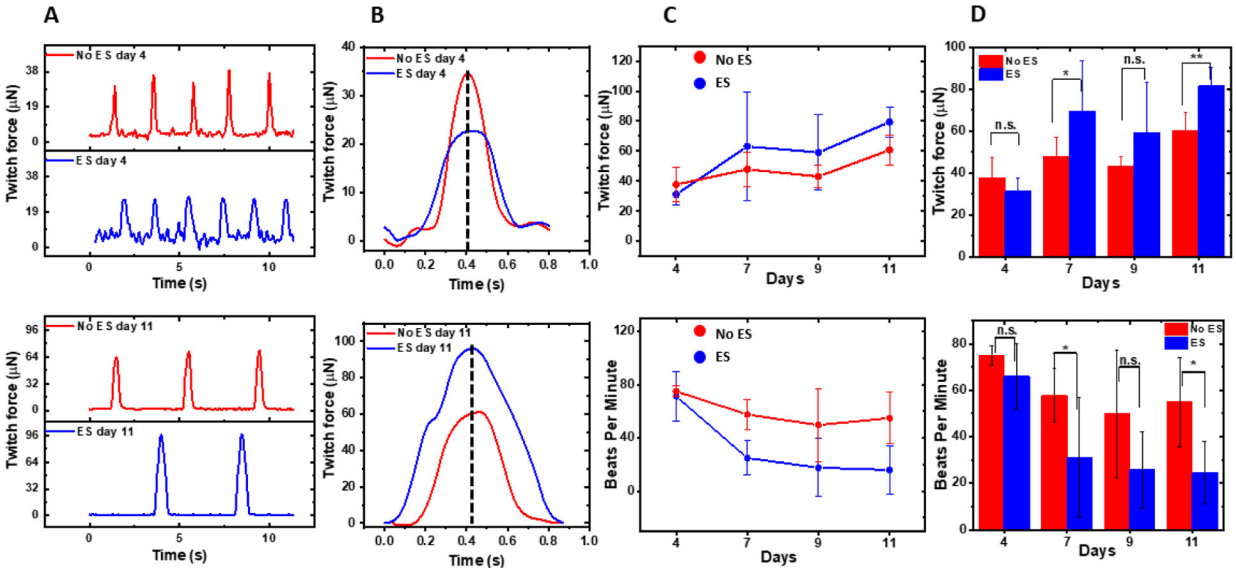

Figure 7. Twitch force and beating rate of the hECTs.

(A) The typical recordings of the twitch force-time traces without (red color) and with ES (blue color) at day 4 (top panel) and day 11 (bottom panel). (B) The comparison of twitch force peak shape. These peaks are the first ones in the traces in (A) and are aligned with their peak positions. (C) The twitch force (top panel) and beating rate (bottom panel) as a function of culture time for hECTs without (red color) and with ES (blue color). The error bars are calculated from the standard deviation of 12 measurements (six samples per day and two repeats per sample). (D) Statistical analysis of the twitch force (top panel) and beating frequency (bottom panel) with N=12. The measurements were conducted at 25 °C.